MOLECULAR
METABOLISM

# Hypothalamic free fatty acid receptor-1 regulates whole-body energy balance

Check for updates

Nathalia R.V. Dragano [1,2,3,*,10], Edward Milbank [1,2,11], Roberta Haddad-Tóvolli [4], Pablo Garrido-Gil [5,6], Eva Nóvoa [1,2], Marcos F. Fondevilla [1,2], Valentina Capelli [1,2], Ariane Maria Zanesco [3], Carina Solon [3], Joseane Morari [3], Leticia Pires [3], Ánxela Estevez-Salguero [1,2], Daniel Beiroa [1,2], Ismael González-García [1,2], Olga Barca-Mayo [1], Carlos Diéguez [1,2], Ruben Nogueiras [1,2], José L. Labandeira-García [5,6], Elisabeth Rexen Ulven [7], Trond Ulven [7], Marc Claret [4,8,9], Licio A. Velloso [3], Miguel López [1,2,**]

## ABSTRACT

**Objective:** Free fatty acid receptor-1 (FFAR1) is a medium- and long-chain fatty acid sensing G protein-coupled receptor that is highly expressed in the hypothalamus. Here, we investigated the central role of FFAR1 on energy balance.

**Methods:** Central FFAR1 agonism and virogenic knockdown were performed in mice. Energy balance studies, infrared thermographic analysis of brown adipose tissue (BAT) and molecular analysis of the hypothalamus, BAT, white adipose tissue (WAT) and liver were carried out.

**Results:** Pharmacological stimulation of FFAR1, using central administration of its agonist TUG-905 in diet-induced obese mice, decreases body weight and is associated with increased energy expenditure, BAT thermogenesis and browning of subcutaneous WAT (sWAT), as well as reduced AMP-activated protein kinase (AMPK) levels, reduced inflammation, and decreased endoplasmic reticulum (ER) stress in the hypothalamus. As FFAR1 is expressed in distinct hypothalamic neuronal subpopulations, we used an AAV vector expressing a shRNA to specifically knockdown *Ffar1* in proopiomelanocortin (POMC) neurons of the arcuate nucleus of the hypothalamus (ARC) of obese mice. Our data showed that knockdown of *Ffar1* in POMC neurons promoted hyperphagia and body weight gain. In parallel, these mice developed hepatic insulin resistance and steatosis.

**Conclusions:** FFAR1 emerges as a new hypothalamic nutrient sensor regulating whole body energy balance. Moreover, pharmacological activation of FFAR1 could provide a therapeutic advance in the management of obesity and its associated metabolic disorders.

## 1. INTRODUCTION

Free fatty acid receptor-1 (FFAR1), also known as GPR40, is a member of the class A of G protein-coupled receptor (GPCR) family that is activated in response to medium- and long-chain fatty acids [1]. Originally, it was described as coupled with Gq protein, activating signal transduction through phospholipase C, and leading to increased intracellular levels of inositol trisphosphate and calcium ($Ca^{2+}$) [2]. However, under certain conditions, it can also transduce signals through other G proteins such as Gs, Gi/o or G12/13, revealing a tissue- and ligand-specific pattern of signal transduction [2—6]. Early studies revealed that FFAR1 is highly expressed in pancreatic beta-cells, and its activation amplifies glucose-stimulated insulin secretion [2]. These findings encouraged the development of agonists that were tested in clinical trials, revealing the effectiveness of using pharmacological agonists of FFAR1 to treat type 2 diabetes mellitus (T2D) [7—9]. The hypothalamus has been identified to also express considerable amounts of FFAR1 [10—13]. Hypothalamic neurons act as sensors for

[1]Department of Physiology, CiMUS, University of Santiago de Compostela, Santiago de Compostela, 15782, Spain [2]CIBER Fisiopatología de la Obesidad y Nutrición (CIBEROBN), 15706, Spain [3]Laboratory of Cell Signaling-Obesity and Comorbidities Research Center, University of Campinas, Campinas, Brazil [4]Neuronal Control of Metabolism (NeuCoMe) Laboratory, Institut d'Investigacions Biomèdiques August Pi i Sunyer (IDIBAPS), Barcelona, Spain [5]Department of Morphological Sciences, CiMUS, University of Santiago de Compostela, Santiago de Compostela, Spain [6]CIBER Enfermedades Neurodegenerativas (CIBERNED), 28029, Santiago de Compostela, Spain [7]Department of Drug Design and Pharmacology, University of Copenhagen, 2100 Copenhagen, Denmark [8]CIBER Diabetes y Enfermedades Metabólicas Asociadas (CIBERdem), 08036, Spain [9]Faculty of Medicine, Universitat de Barcelona, Barcelona, Spain

[10] Current address: Institute of Experimental Genetics — German Mouse Clinic — Neuherberg, Germany; German Center for Diabetes Research (DZD) — Neuherberg, Germany.

[11] Current address: Molecular Cell Biology, Institute for Theoretical Medicine, Medical Faculty, University of Augsburg, Augsburg, Germany.

*Corresponding author. Department of Physiology, CiMUS, University of Santiago de Compostela, Santiago de Compostela, 15782, Spain. E-mail: nathalia.dragano@helmholtz-munich.de (N.R.V. Dragano).

**Corresponding author. Department of Physiology, CiMUS, University of Santiago de Compostela, Santiago de Compostela, 15782, Spain. E-mail: m.lopez@usc.es (M. López).

whole-body energy balance providing signals that regulate caloric intake and energy expenditure [14—16]. Pharmacological interventions that reduce food intake and increase energy expenditure could provide an advance in the treatment of obesity and its comorbidities [14—16]. Here, we first explored in depth the role of FFAR1 on the hypothalamic mechanisms regulating energy balance by treating mice with TUG-905, a FFAR1-specific agonist with preserved activity in the murine receptor orthologues and with a selectivity of at least 1000-fold over FFAR4 [17]. We showed that most of the catabolic effects promoted by this compound are due to increased brown adipose tissue (BAT) thermogenesis and subcutaneous white adipose tissue (sWAT) browning. Next, as proopiomelanocortin (POMC)-expressing neurons in the arcuate nucleus of the hypothalamus (ARC) are a key neuronal population implicated in energy balance control [18], we silenced the expression of FFAR1 specifically in this cell population. POMC *Ffar1* knockdown mice showed increased body mass gain associated with hyperphagia and a worsening of hepatic insulin sensitivity and steatosis. Thus, hypothalamic FFAR1 plays an important role in regulating whole-body energy balance and could be regarded as a new and promising target for the treatment of obesity and metabolic comorbidities.

## 2. MATERIAL AND METHODS

### 2.1. Animal care and mouse lines
Adult male C57BL/6J mice (weight 20—25 g, age 6—8 weeks) were housed under controlled conditions of light (12-h light/dark cycle), temperature (21 ± 2 °C), and humidity (40%). Mice were fed on a high-fat diet (HFD, 60% fat, 20% carbohydrate, 20% protein, 5.21 kcal/g; D12492; Research Diets, Inc) and tap water ad libitum, unless otherwise indicated. Mice expressing Cre recombinase under the control of the POMC promoter were obtained from The Jackson Laboratory (Tg (Pomc1-cre)16Lowl/J Strain #005965) and used to investigate the role of FFAR1 specifically in this neuronal population. Mice were housed collectively in groups of 5 per cage for 8 weeks before the onset of experiments, when they were transferred to individual housing. Animal experiments presented in this manuscript were approved by the USC Ethical Animal Committee (Project ID 15010/14/006 and 15012/2020/010). All the experiments were performed in agreement with the Rules of Laboratory Animal Care and International Law on Animal Experimentation.

### 2.2. FFAR1 expression in the hypothalamus
To determine whether FFAR1 expression was modulated by different nutritional and dietary conditions, adult male C57BL/6J mice fed a HFD were fasted overnight (12 h) and refed ad libitum for 4 h.

### 2.3. FFAR1 synthetic agonist
The selective FFAR1 agonist TUG-905 was synthesized as previously described [19].

### 2.4. Intracerebroventricular cannulation and treatments
Lateral intracerebroventricular (ICV) administration was carried out in male C57BL/6J under diet-induced obesity (DIO) conditions, as previously shown [20]. After surgery, the animals were single housed and given at least 4 days to recover. Obese mice were infused with 2 µl of either vehicle (10% DMSO, 90% saline) or TUG-905 (0.5 µg/µl) for 7 consecutive days, once a day, 2 h before dark phase. Because daily central manipulation of mice with TUG-905 ICV infusion could interfere with continued monitoring of energy expenditure, brain infusion

cannulae were placed into the lateral ventricle; a catheter tube was connected from the cannula to an osmotic minipump (Model 2002; ALZET Osmotic Pumps). The osmotic minipumps were inserted in a subcutaneous pocket on the dorsal surface of the animal [20]. These pumps had a flow rate of 0.5 µl/h during 14 days (Vehicle or TUG-905 at 1 µg/day).

### 2.5. Stereotaxic microinjection of adeno-associated virus vectors
POMC-Cre mice fed on a HFD for 8 weeks were anesthetized with ketamine/xylazine cocktail (15 mg/kg and 3 mg/kg, respectively) and placed in a stereotaxic frame for subsequent adeno-associated virus (AAV) injection into the ARC. An AAV vector expressing a shRNA targeting *Ffar1* (AAV1-CMV-DIO-TATAlox-*Gfp*-U6-sh(m *Ffar1*); SignaGen Laboratories) was used to knockdown *Ffar1* in the POMC neurons from ARC. AAV vectors expressing a scramble shRNA sequence (AAV1-CMV-DIO-TATAlox-*Gfp*-U6-sh (Scramble); SignaGen Laboratories), were used as control. Viral concentrations were $1.0 \times 10^{13}$ vg/ml. 0.5 µl of AAV were administered bilaterally into the ARC, using a 33-gauge needle connected to a 1 ml syringe (Neuro-Syringe, Hamilton) according to the following coordinates: 1.5 mm posterior to the Bregma, ±0.2 mm lateral to midline, and 5.8 mm below the surface of the skull. Before needle retraction, a 10-min time lapse was allowed to prevent a backflow through the needle track, as previously shown [20,21]. Experiments were conducted at least 3 weeks after injections to ensure AAV expression.

### 2.6. Temperature measurements
Body temperature was recorded twice before the ICV treatments with a rectal probe connected to a digital thermometer (BAT-12: Microprobe-Thermometer). Skin temperature surrounding BAT was recorded with a B335 compact infrared thermal imaging camera (FLIR) and analyzed with FLIR Tools software (FLIR Systems), as shown [22,23].

### 2.7. Indirect calorimetry
Mice were analyzed for energy expenditure (EE), respiratory exchange ratio (RER) and spontaneous locomotor activity (LA) using a calorimetric system (LabMaster; TSE Systems), as previously described [22—24].

### 2.8. Hepatic insulin signaling
To study insulin signaling specifically in the liver, mice were fasted for 6 h and then anesthetized with ketamine/xylazine cocktail (15 mg/kg and 3 mg/kg, respectively). The abdominal cavity was opened, a small fragment of liver was excised (baseline condition) and then, 125 µl of an insulin bolus containing 5 units of insulin (Actrapid, NovoNordisk) diluted in saline was injected into the inferior cava vein. Samples of liver were excised 2 min after injection (insulin injected condition) [25,26].

### 2.9. Sample processing
Samples from the cortex, mediobasal hypothalamus (MBH), ARC, lateral hypothalamic area (LHA), ventromedial nucleus of the hypothalamus (VMH), liver, skeletal muscle, BAT, gonadal adipose tissue (gWAT) and sWAT were dissected for the different experimental settings. Tissues were kept at −80 °C until their analysis.

### 2.10. Serum biochemical analysis
Leptin circulating levels were measured using a mouse enzyme-linked immunosorbent assay kit (Millipore). Cholesterol, triglycerides (Spinreact), free-fatty acids (FFA) and non-esterified fatty acids (NEFA)

(WAKO) were measured by spectrophotometry in a Multiskan GO spectrophotometer (Invitrogen-ThermoFisher).

## 2.11. HPLC chromatography

BAT samples were dissected on a chilled plate, and immediately flash-frozen in dry ice before being stored at $-80\ ^\circ C$ until further analysis. The frozen tissue was subsequently homogenized, sonicated, and centrifugated at 14,000 g for 20 min at 4 $^\circ C$. The resulting supernatant fraction was filtered and then injected into a high-performance liquid chromatography (HPLC) system (Shimadzu LC Prominence; Shimadzu Corporation) [27,28]. To separate norepinephrine (NE), dopamine (DA), and serotonin (5-HT), a reverse-phase analytical column (Waters Symmetry 300C18; Waters) was employed. The mobile phase consisted of a 10% MeOH solution (pH = 4) containing 70 mM $KH_2PO_4$, 1 mM octanesulfonic acid, and 1 mM EDTA, delivered at a flow rate of 1 ml/min. Detection of the neurotransmitters was achieved using a coulometric electrochemical detector (ESA Coulochem III; Thermo Scientific). The first and second electrodes of the analytical cell were set at $+50$ mV and $+350$ mV, respectively, while the guard cell was set at $-100$ mV. Data acquisition and processing were performed using the Shimadzu LC solution software (Shimadzu Corporation). The concentrations of the neurotransmitters were expressed as pg/mg of wet tissue, as shown [27,28].

## 2.12. Histological analysis

BAT and sWAT samples were processed as shown [21,29,30]. For the adipocyte area, images were analyzed with ImageJ Software (NIH). BAT sections were used for immunohistochemistry detection of uncoupling protein 1 (UCP1). UCP1-positive cells were quantified with FRIDA image analysis software, as described elsewhere [29]. Hepatic lipid content was analyzed by Oil Red O staining, as previously described [21,25,29]. Lipids in Oil Red O-stained sections were quantified using ImageJ software (NIH). Three pictures per each image section were analyzed. All analyzed values are represented with respect to control (100%). Direct detection of GFP fluorescence was performed after perfusion of the animals, on 20 μm brain sections. Images were taken with a fluorescence microscope Olympus IX51 [21,31,32].

## 2.13. RNAscope

Mice were perfused via transcardiac injection with 0.9% saline followed by 4% paraformaldehyde (PFA; pH 7.4). The brains were dissected and post-fixed in 4% PFA at 4 $^\circ C$ for 24 h, and cryoprotected by a sequence of 10—30% sucrose in $1\times$ phosphate buffered saline (PBS, pH 7.4) at 4 $^\circ C$ until the tissue sunk to the bottom of the tube. Brain sections (20 μm) were obtained on a cryostat (Leica CM 1950) and collected in series (one every 4 sections) in SuperFrost UltraPlus Adhesion slides (ThermoFisher), air-dried at room temperature (RT) and subsequently stored at $-80\ ^\circ C$ to preserve RNA until further processing. Fluorescent in situ hybridization for the simultaneous detection of Pomc, Gfp and Ffar1 mRNA was performed using RNA-Scope. All reagents were purchased from Advanced Cell Diagnostics (ACD). The Gfp probe (Cat. Nº 409011-C3) contained 20 oligo pairs and targeted region 407—1427 (NM_010234.2) of the Gfp transcript. The Pomc probe (Cat No. 314081-C1) contained 10 oligo pairs and targeted region 19-995, (NM_008895.3) of the Pomc transcript. The Ffar1 probe (Cat. Nº 464311-C2) constituted 18 oligo pairs and targeted region 19—882 of the Ffar1 transcript (NM_194057.2). All incubation steps were performed at either at 60 $^\circ C$ or 40 $^\circ C$ using the ACD HybEz hybridization system (Cat. Nº 321720). From each animal, one section from the same region of the brain was also mounted as negative control probe to enable subsequent calculation of background. Slides were washed in PBS, baked at 60 $^\circ C$ for 30 min and post-fixed with 4% PFA for 15 min. Sections were then dehydrated and baked for a second time for 30 min at 60 $^\circ C$ and subsequentially submerged into boiling (98.5—100 $^\circ C$) Target Retrieval (Cat. Nº 322000) for 5 min, followed by two brief rinses in MilliQ-purified water. The slides were quickly dehydrated in 100% ethanol and allowed to air dry for 5 min. A hydrophobic barrier was then created around the sections using an ImmEdge hydrophobic barrier pen (Cat. Nº H-4000; Vector laboratories). Slides were then placed into RNAScope holder and sections were treated with Protease III for 30 min at 40 $^\circ C$. The subsequent steps, i.e., hybridization of the probes and the amplification and detection steps, were performed according to the manufacturer's protocol for RNAscope Multiplex Fluorescent Assay. The color module chosen for the experiment finally labeled the Pomc probe with Atto 550, the Gfp probe with Atto 647, and the Ffar1 probe with Atto 488. Sections were counterstained with DAPI and coverslipped with ProLong Gold Antifade Mountant (Cat. Nº P36930; ThermoFisher) and stored in the dark at 4 $^\circ C$ until imaging.

Images were captured using a confocal Leica DM 2500 microscope, equipped with a $40\times/1.15$ oil objective, and using a zoom of $2\times$. Z-stacks of 1 μm of the ARC were captured bilaterally from 5 rostral to caudal sections per animal (n = 3/4 animals per group). Laser intensities for the three probe channels were kept constant throughout the entire image acquisition. Images were imported into Fijii (NIH) where maximum intensity projections were made. To acquire the minimum intensity value for analyzing the expression of Ffar1, the threshold for probe recognition was calculated as the mean cell intensity present in the negative control sections $+3xSD$. All labeling above this value was considered as true signal. Brightness (min = 10/max = 150) and threshold (default/BW) (35-200) were adjusted in all images. For quantification, each Pomc+/Gfp+ neuron per section were manually selected and the amount of Ffar1 particles were analyzed.

## 2.14. Western blot analysis

Western blot was performed as previously described [20—23,32]. The protein lysates were subjected to SDS-PAGE, electrotransferred to PVDF membranes with a semidry blotter and probed with primaries antibodies (Supplementary Table 1) as previously shown [20—23,32]. Autoradiographic films were scanned, and the bands signal was quantified by densitometry using ImageJ (NIH). β-Actin or α-tubulin served as a loading control, and control values were normalized to 100%. Representative images for all proteins are shown with all bands for each picture derived from the same gel, although they may be spliced for clarity. In several cases, proteins were assayed in the same membranes, therefore, some of the β-actin or α-tubulin were common in their representative panels. This happens in Figure 3I: selected α-tubulin bands for PGC1α and DIO2 and Figure 7C: selected β-actin bands for pSTAT3 and SOCS3 (Supplementary Data: Uncropped Gels File).

## 2.15. Real-time PCR

RNA was extracted using Trizol® reagent (Invitrogen) according to the manufacturer's instructions. Total RNA (1—2 μg) was used for each RT reaction, and cDNA synthesis was performed using the SuperScript™ First-Strand Synthesis System (Invitrogen) and random primers, also following the supplier's protocol. Real-time PCR (TaqMan) was performed as previously described [20—23,32]. For data analysis, the

input value of gene expression was standardized to the *Hprt* value for the sample group and expressed as a comparison with the average value for the control group. All samples were run in duplicate, and the average values were calculated. The references of all primers used are shown in Supplementary Table 2.

## 2.16. Data analysis and statistics

Data are expressed as mean ± SEM; when data are normalized, they are expressed as a percentage of the appropriate controls. Statistical significance was assessed using two-sided (at least one-sided is specified) Student's t-test (for comparison of two groups), one-way ANOVA, two-way ANOVA or Mixed effect analysis, followed of Bonferroni's multiple comparisons (for comparison involving more than two groups) or ANCOVA (calorimetric analyses). P < 0.05 was considered significant. Data analysis was performed using Prism 8.0.2 Software (GraphPad).

## 3. RESULTS

### 3.1. Hypothalamic FFAR1 was regulated by nutritional status

Previous studies have shown that FFAR1 is preferentially expressed in the pancreatic beta cells and the brain [1]. In situ hybridization was employed to examine hypothalamic FFAR1 expression. Our results revealed robust FFAR1 signal, with the highest levels observed in the ARC, followed by the VMH, and finally the lateral hypothalamic area (LHA) (Figure 1A, B). Next, we explored whether hypothalamic FFAR1 expression was modulated upon nutritional interventions. Our data showed that while the consumption of HFD increased the expression of hypothalamic FFAR1 (Figure 1C, D), mice on fasting state displayed reduced levels (which were not recovered after 4 h of refeeding; Figure 1E, F). These findings indicated that FFAR1 was decreased under conditions of nutrient deficiency and upregulated upon energy excess.
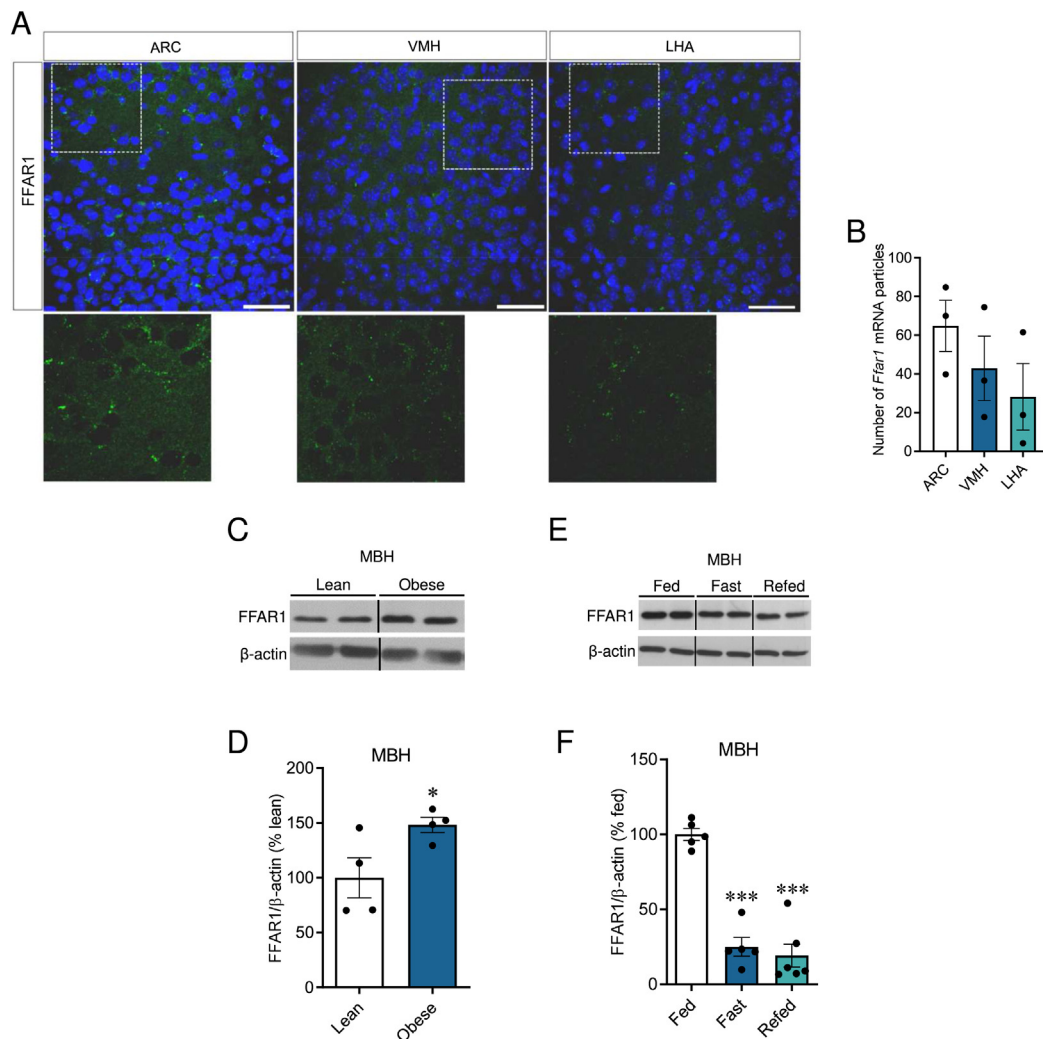


**Figure 1:** Hypothalamic expression and regulation of FFAR1. (A) Representative confocal images (40×) and (B) quantification of in situ hybridization of FFAR1 mRNA (green) in coronal sections of the hypothalamus mice (n = 3 mice/group). Nuclear counterstaining is shown in blue. Scale bar: 25 μm. (C) Representative immunoblot images and (D) densitometry quantification of FFAR1 expression in the mediobasal hypothalamus (MBH) from adult male C57BL/6J lean and obese mice (4 weeks on HFD) (n = 4/group). (E) Representative immunoblot images and (F) densitometry quantification of FFAR1 expression in the MBH of fed, fasted and refed (12 h overnight fasting followed by 4 h of refeeding) adult male C57BL/6J mice (n = 5–6/group). Data are expressed as MEAN ± SEM. Statistical significance was determined by one-way ANOVA (B and F) or Student's t-test (D); *P < 0.05 and ***P < 0.001 *vs.* Lean or Fed.
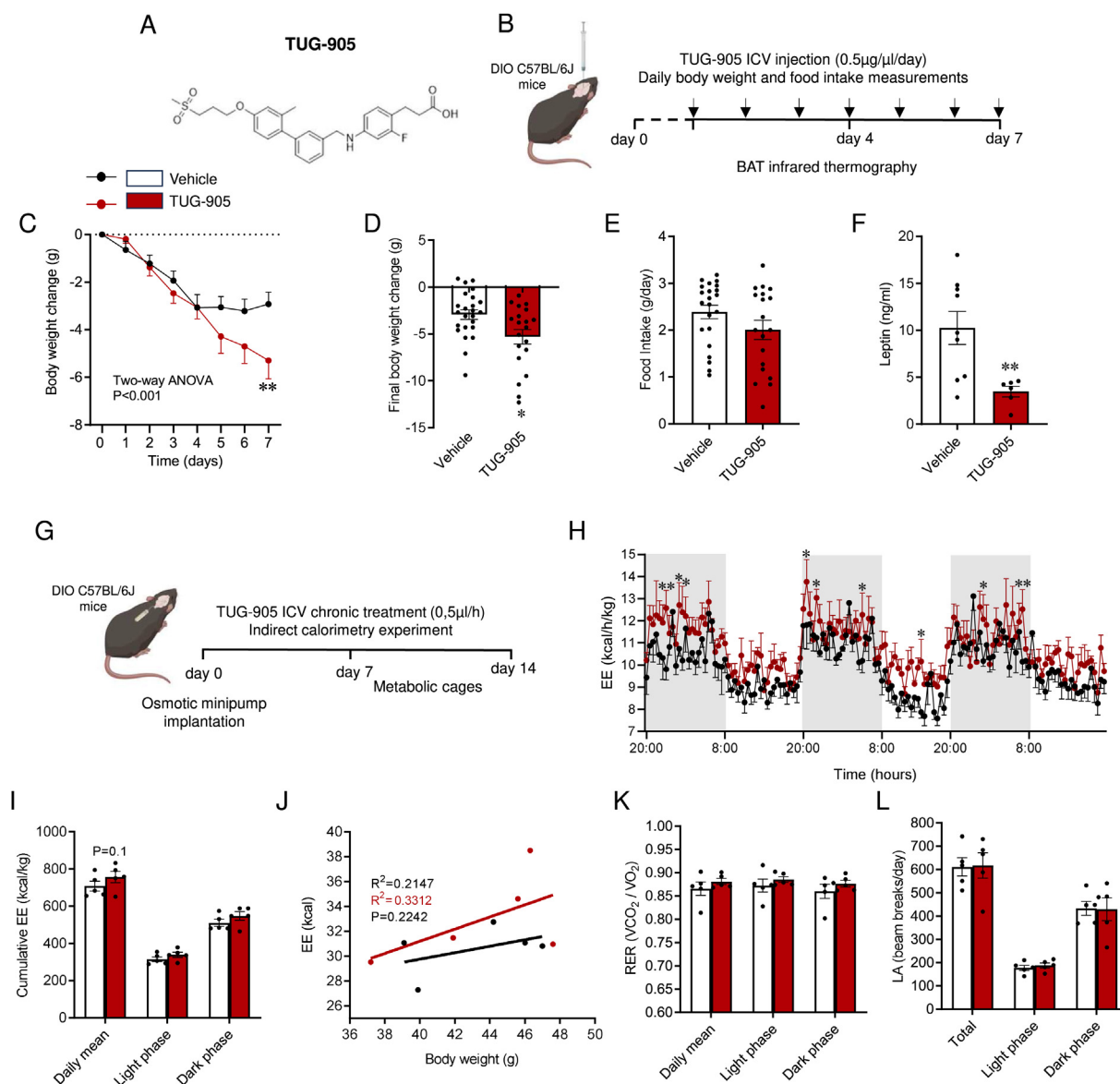
**Figure 2:** Effect of central TUG-905 administration on energy balance in obese mice. (A) TUG-905 chemical structure. (B) Schematic illustration of experimental timeline for TUG-905 daily bolus. TUG-905 (0.5 μg/μl) was injected by intracerebroventricular (ICV) administration once a day for 7 days. Body weight and food intake were measured daily. BAT temperature was measured at day 0 (the day before TUG-905 ICV treatment), day 4 and day 7 of the experiment. (C) Body weight change during the 7 days experimental period, (D) final body weight change after 7 days of TUG-905 ICV treatment (n = 20−24 mice/group), (E) daily food intake (n = 19−22 mice/group; 3 mice spilled food into the cage and feeding could not be recorded) and (F) circulating leptin levels (n = 6−9 mice/group) of vehicle and TUG-905 ICV-treated DIO mice. (g) Schematic illustration of the experimental strategy for continuous mini-pump TUG-905 ICV administration. Eight-week-old C57Bl/6J mice were fed with HFD for 8 consecutive weeks. Afterwards, these mice were submitted to an implantation of an osmotic minipump loaded with TUG-905 and transferred to the indirect calorimetry system for measurements after 7 days of surgery recovery. (H) Energy expenditure (EE) during dark and light phases, (I) cumulative EE, (J) ANCOVA analysis of EE using body weight as a covariate, (K) respiratory exchange ratio (RER) and (I) spontaneous locomotor activity (LA) (n = 5 mice/group) of vehicle and TUG-905 ICV-treated DIO mice. Data are expressed as MEAN ± SEM. Statistical significance was determined by two-way ANOVA (C and H), ANCOVA (J) or Student's t-test (D, E, F, I, K, and L); *P < 0.05 and **P < 0.01 *vs.* vehicle.

## 3.2. Central pharmacological activation of FFAR1 induced body weight loss in DIO mice

TUG-905 (Figure 2A) is a potent and specific agonist of FFAR1 [10,19]. Daily ICV infusion of TUG-905 for 7 days (Figure 2B) promoted feeding-independent body weight loss (Figure 2C−E and Suppl. Fig. 1A), associated with lower circulating levels of leptin (Figure 2F), usually indicative of reduced adiposity. Because daily central manipulation of mice with TUG-905 ICV infusion could interfere with continued monitoring of energy expenditure (opening of the cages for ICV injection, handling, etc.), an osmotic minipump loaded with TUG-905 was implanted in a subgroup of mice. After a resting period of 7 days, mice were transferred to an indirect calorimetry system for measurements (Figure 2G). During the whole period, TUG-905-treated mice presented a tendency to increase energy expenditure (Figure 2H−J), while no modification of RER (Figure 2K) and LA (Figure 2L) were detected.

## 3.3. Central pharmacological activation of FFAR1 induced BAT thermogenesis and browning of WAT

Bearing in mind the lack of effects on food intake associated to central TUG-905-induced body weight loss, we next aimed to
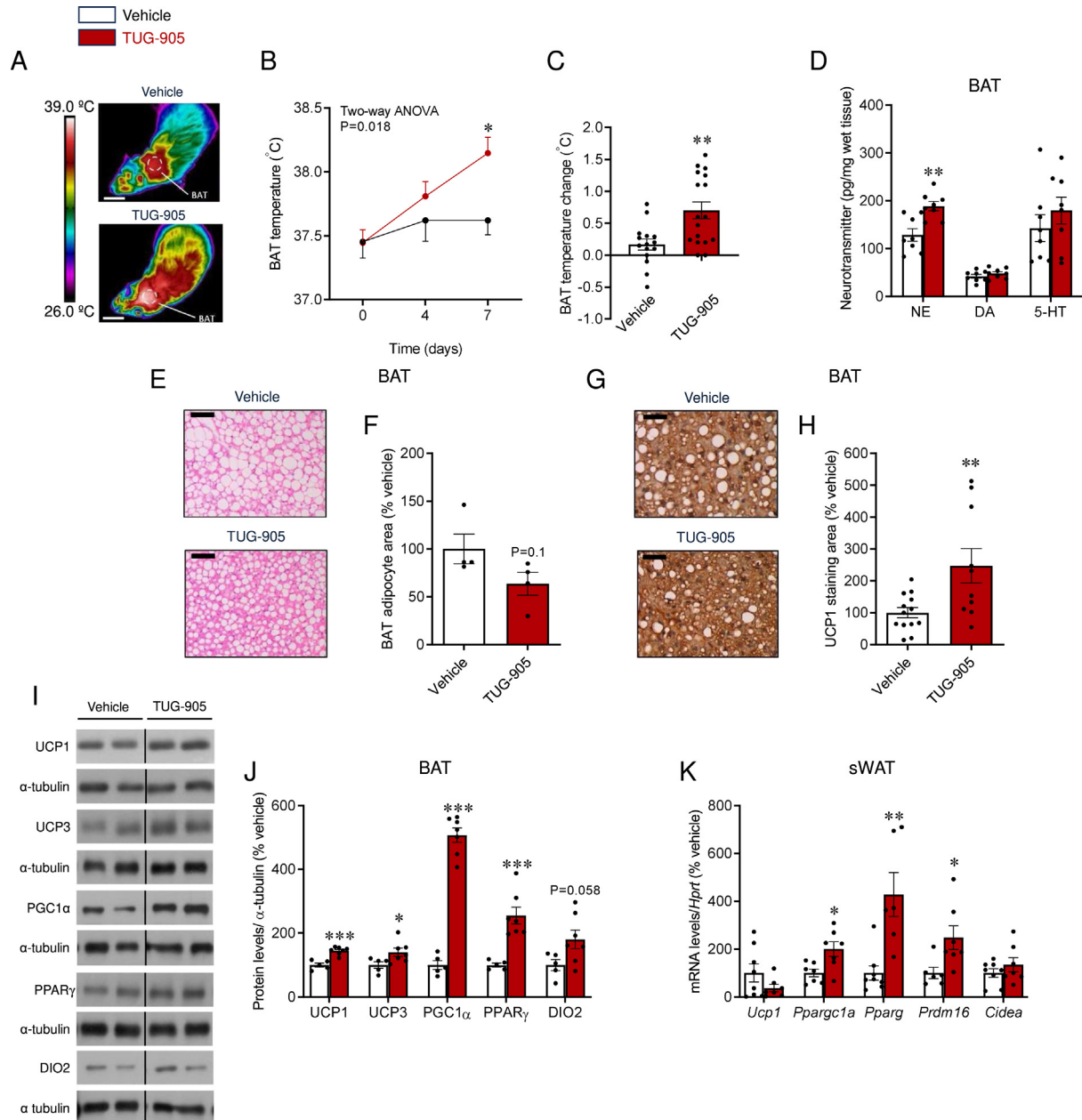
**Figure 3:** Effect of central TUG-905 administration on BAT and WAT in obese mice. (A) Representative BAT thermographic images (scale bars represent 1 cm), (B) BAT temperature quantification at the experimental days 0, 4 and 7, (C) BAT temperature change between experimental days 0 and 7 (n = 15−17 mice/group), (D) BAT neurotransmitters levels (n = 8 mice/group), (E) representative microphotographs of H&E staining (20X, scale bar: 200 μm), (F) adipocyte area (n = 4 mice/group), (G) representative UCP1 staining in the BAT (20X, scale bar: 200 μm), (H) BAT UCP1 stained area (n = 10−13 mice/group), (I) representative immunoblot images, (J) densitometry quantification of thermogenic markers in the BAT (n = 5−7 mice/group) and (K) mRNA levels of thermogenic markers in the sWAT (n = 6−8 mice/group) of vehicle and TUG-905 ICV-treated DIO mice. Data are expressed as MEAN ± SEM. Statistical significance was determined by two-way ANOVA (B) or Student's t-test (C, D, F, H, J, and K); *P < 0.05, **P < 0.01, ***P < 0.001 *vs.* vehicle.

investigate its potential role modulating thermogenic mechanisms. Our data showed that ICV TUG-905 promoted an increase in inter-scapular BAT temperature (Figure 3A−C), with no changes in rectal temperature (data not shown). In keeping with this, TUG-905 treated mice displayed higher levels of NE in the BAT, indicating of higher noradrenergic, and therefore sympathetic, tone (Figure 3D). No changes were observed in other analyzed neurotransmitters, such as DA or 5-HT (Figure 3D).

Histological analyses of BAT revealed smaller lipid droplets and reduced adipocyte area upon central TUG-905 treatment (Figure 3E, F),

as well as an increased UCP1 content (Figure 3G, H), which was accompanied by the increased expression of all BAT thermogenic markers (Figure 3I, J), namely UCP1, uncoupling protein 3 (UCP3), peroxisome proliferator-activated receptor gamma coactivator 1-alpha (PGC1α), peroxisome proliferator-activated receptor gamma (PPARγ) and iodothyronine deiodinase 2 (DIO2). Central TUG-905 treatment also induced browning of sWAT, as shown by the increased mRNA levels of thermogenic markers, such as *Pparg*, *Ppargc1a,* and *PR* domain containing 16 (*Prdm16*) (Figure 3K). Central administration of TUG-905 reduced liver weight (Vehicle: 1.21 ± 0.05 g; TUG-905:
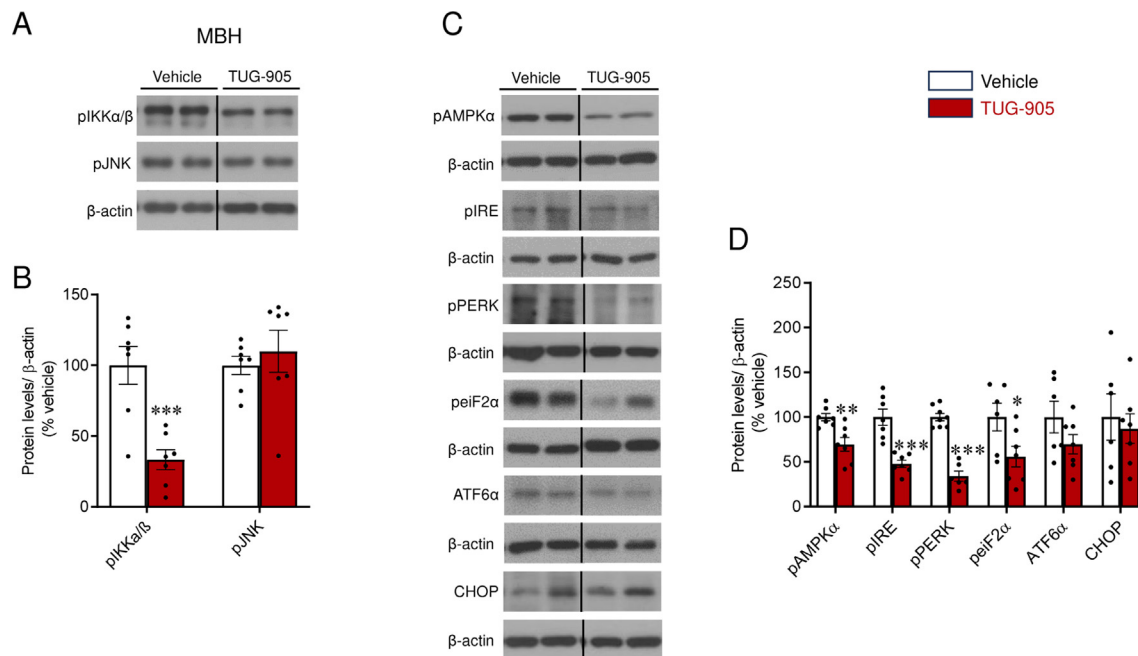
**Figure 4:** Effect of central TUG-905 administration on the hypothalamus of obese mice. (A) Representative immunoblot images and (B) densitometry quantification of protein levels of inflammation markers in the MBH (n = 7 mice/group) of vehicle and TUG-905 ICV-treated DIO mice. (C) Representative immunoblot images and (D) densitometry quantification of protein levels of pAMPK and ER stress markers in the MBH (n = 6−8 mice/group) of vehicle and TUG-905 ICV-treated DIO mice. Data are expressed as MEAN ± SEM. Statistical significance was determined by Student's t-test *$P < 0.05$, **$P < 0.01$, ***$P < 0.001$ *vs.* vehicle.

1.002 ± 0.023 g; $P < 0.01$) without a significant impact on steatosis (Suppl. Figs. 1B and C). Additionally, it led to a decrease in blood non-esterified fatty acids, while unchanging plasmatic triglycerides and cholesterol (Suppl. Figs. 1D−F).

### 3.4. Central pharmacological activation of FFAR1 decreased hypothalamic inflammation, AMPK and ER stress

Recent findings have linked reduced hypothalamic inflammation, as well as AMP-activated protein kinase (AMPK) and ER stress to increased BAT activation [15,21,24,31,33]. Our data showed that central TUG-905 promoted similar changes, as demonstrated by reduced phosphorylation of IKKα/β (pIKKα/β) with no changes in phosphorylated c-Jun N-terminal kinase (pJNK) protein levels (Figure 4A, B), as well as decreased levels of phosphorylated AMPK alpha (pAMPKα) and several molecular markers of the unfolded protein response (UPR), such as phosphorylated inositol-requiring kinase 1 (pIRE), phosphorylated protein kinase RNA-like endo-plasmic reticulum kinase (pPERK) and phosphorylated eukaryotic initiation Factor 2 (peiF2α) (Figure 4C, D) in the MBH. No changes were detected in the protein levels of either activating transcription factor 6 alpha (ATF6α) or C/EBP homologous protein (CHOP) (Figure 4C, D).

### 3.5. Knockdown of *Ffar1* in POMC neurons promoted hyperphagia and body mass increase

To explore the neuron-specific roles of FFAR1 in the mouse hypo-thalamus, we stereotaxically delivered in the ARC of DIO POMC-Cre mice an AAV expressing *Ffar1* shRNA in a Cre-dependent manner; this allowed to knockdown *Ffar1* in POMC neurons (Figure 5A), a key population modulating mainly food intake and energy expenditure [18]. AAV infection efficiency in the ARC was assessed by expression

of green fluorescent protein (GFP) (Figure 5B and Suppl. Fig. 2A). FFAR1 depletion in MBH (ARC + VMH) was initially confirmed by western blot, which showed a significant 27% reduction in the knockdown group (Figure 5C, D). For a more precise analysis, we performed fluorescence in situ hybridization (Figure 5E−M), specif-ically in POMC neurons. Using this method, *Ffar1* knockdown effi-ciency was shown to be ∼66% (Figure 5M), confirming the efficiency of the procedure. Of note, the total number of infected POMC neurons is comparable between the *Ffar1* knockdown and control groups (Suppl. Fig. 2B).

Metabolic phenotyping upon AAV injection revealed that the knock-down of *Ffar1* in POMC neurons promoted body weight gain (Figure 6A, B and Suppl. Fig. 2C), and hyperphagia (Figure 6C, D). Notably, despite the reported role of POMC neurons as modulators of energy meta-bolism [18], no changes in EE (Figure 6E−G) were detected. No dif-ferences were found in either RER (Figure 6H), LA (Figure 6I), BAT temperature (Figure 6J−K) or the expression of thermogenic proteins in BAT (Figure 6L, M), indicating that the increase body weight was due to increased feeding.

### 3.6. Knockdown of *Ffar1* in POMC neurons increased hypothalamic ER stress and reduced leptin signaling

Next, we aim to uncover the key hypothalamic signaling pathways involved in the elevated food intake following POMC-specific knock-down of *Ffar1*. Our data showed that the changes in food intake promoted by the knockdown of *Ffar1* in POMC neurons were accompanied by increased expression of hypothalamic ER stress markers (Figure 7A, B) and reduced hypothalamic phosphorylated signal transducer and activator of transcription 3 (pSTAT3), but not suppressor of cytokine signaling 3 (SOCS3) expression (Figure 7C, D), suggesting diminished leptin signaling.
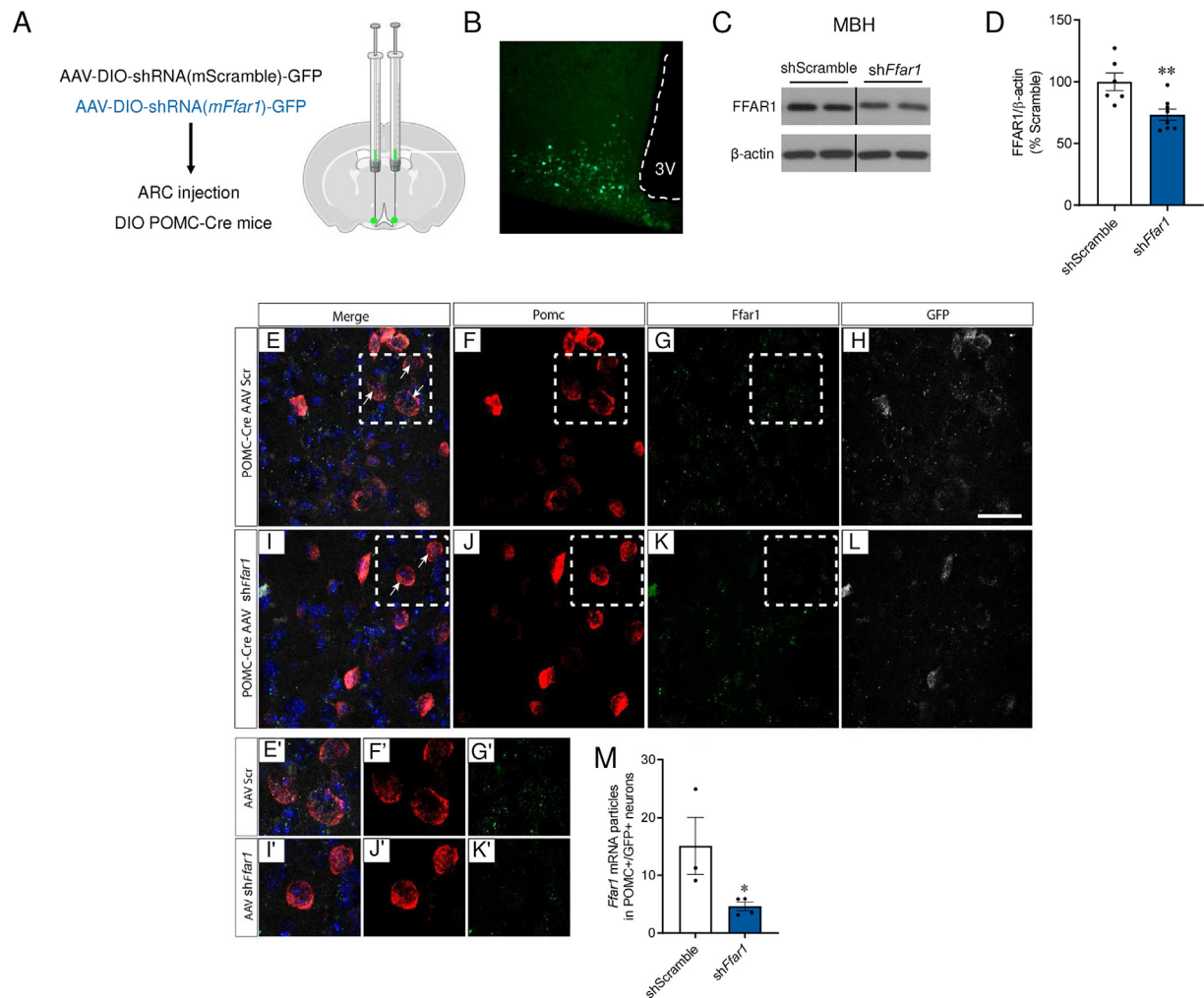
**Figure 5:** Effect of stereotaxic delivery of AAV encoding shRNA against *Ffar1*. (A) Schematic illustration of AAV vector bilateral injections in the ARC of DIO POMC-Cre mice. (B) Representative photomicrograph of a brain section showing the injection of the viral vectors that encode GFP expression precisely placed in the ARC. (C) Representative immunoblot images, (D) densitometry quantification of FFAR1 expression in the MBH (n = 6–8 mice/group), (E–L) representative confocal images (square areas magnified in E′-K′) and (M) quantification of in situ hybridization of *Pomc* (red), *Ffar1* (green) and *Gfp* (gray) mRNA in coronal sections of the ARC (n = 3–4 mice/group) of POMC-Cre mice treated with AAV encoding shScramble or sh*Ffar1*. Nuclear counterstaining is shown in blue. Scale bar: 25 μm. Data are expressed as MEAN ± SEM. Statistical significance was determined by Student's t-test *$P < 0.05$, **$P < 0.01$ *vs.* shScramble.

### 3.7. Knockdown of *Ffar1* in POMC neurons worsens hepatic insulin sensitivity

POMC *Ffar1* knockdown mice presented hepatic abnormalities, such as tendencies to increased liver weight (Figure 8A) and hepatic fat accretion (Figure 8B, C), as well as impaired hepatic insulin signaling, as demonstrated by impaired insulin-induced AKT phosphorylation (pAKT) in POMC *Ffar1*-KD mice (Figure 8D, E). Together, these data demonstrate that *Ffar1* knockdown in POMC neurons resulted in hyperphagia, and body weight gain, ultimately leading to hepatic insulin resistance, thus worsening the obese and metabolic phenotype induced when fed a HFD.

## 4. DISCUSSION

Here, we show that FFAR1 is expressed in hypothalamic neurons and that it is involved in the regulation of whole-body energy balance and hepatic insulin sensitivity. FFAR1 belongs to the class A GPCR family and was identified as a receptor for medium- and long-chain fatty acids [1]. GPCRs are the largest family of membrane receptors, and up to 34% of all drugs currently approved for the treatment of distinct human diseases target members of this group [34]. Early studies have shown that FFAR1 is highly expressed in pancreatic islets and its activation leads to amplified glucose-induced insulin secretion [2], whereas the opposite occurs as a result of its deletion [35]. Because of the promising results obtained in experimental studies, chemical agonists were developed and tested in patients with T2D, resulting in improved control of blood glucose levels [7–9]. Currently, there are several agonists of FFAR1 under development by pharmaceutical companies [36].

FFAR1 is also expressed in the hypothalamus [11]. In this study, we first showed that FFAR1 is modulated by nutritional status, being increased after HFD exposure and decreased after fasting. Hypothalamic neurons act as sensors of systemic signals that mirror the energy reserves of the entire body [37,38]. In addition to hormones, hypothalamic neuronal signaling is also triggered by nutrients, including fatty acids [14–16]. Early studies have identified intracellular
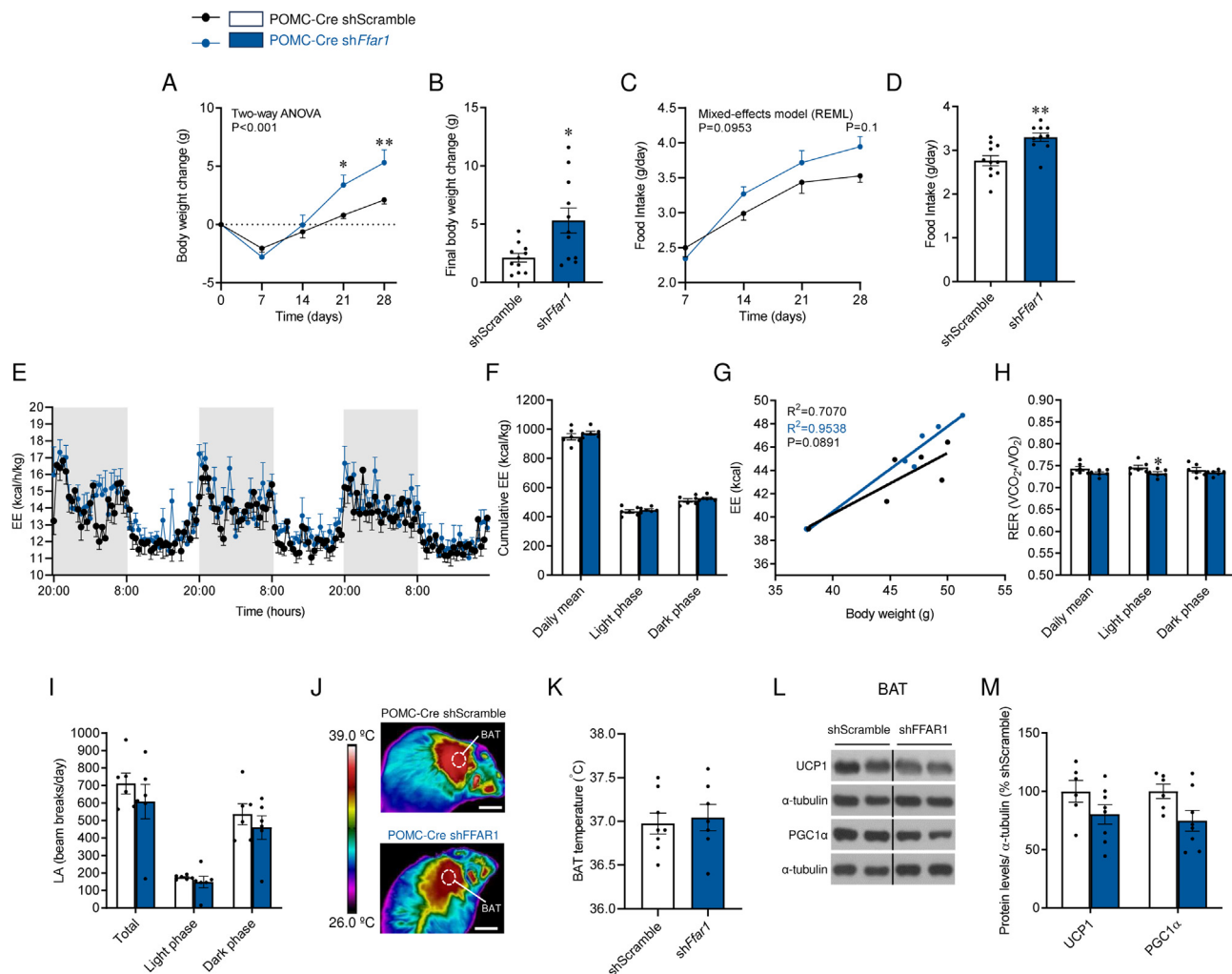
**Figure 6:** Effect of POMC-specific *Ffar1* knockdown on energy balance and BAT. (A) Body weight change (B) final body weight change, (C) daily food intake (D) average food intake (d) (n = 10−11 mice/group), (E) energy expenditure (EE) during dark and light phases, (F) cumulative EE, (G) ANCOVA analysis of EE using body weight as a covariate, (H) respiratory exchange ratio (RER), (I) spontaneous locomotor activity (LA) (h) (n = 6 mice/group), (J) representative BAT thermographic images (scale bars represent 1 cm), (K) average BAT temperature quantification, (L) representative immunoblot images and (M) densitometry quantification of thermogenic markers in the BAT (n = 6−8 mice/group) of POMC-Cre mice treated with AAV encoding shScramble or *shFfar1*. Data are expressed as MEAN ± SEM. Statistical significance was determined by two-way ANOVA (A, E), Mixed-effects model (C), ANCOVA (G) or Student's t-test (B, D, F, H, I, K, and M); *$P < 0.05$ and **$P < 0.01$ *vs.* shScramble.

mechanisms involved in the regulation of energy balance in response to fatty acids acting in the MBH neurons. Following their entrance, long-chain fatty acids (LCFA) are rapidly esterified by LCFA-CoA synthase to form LCFA-CoA [39]. The rise in LCFA-CoA neuronal levels leads to mitochondrial β-oxidation, inducing the release of agouti-related peptide (AgRP) and neuropeptide Y (NPY), thus increasing appetite [40]. Physiologically, this mechanism is active during prolonged fasting and leads to the activation of lipolysis in the adipose tissue, resulting in increased blood levels of FFAs [39]. Further studies have shown that, in addition to the oxidative-based intracellular signaling mechanism, fatty acids could modulate hypothalamic function by activating membrane receptors, such as FFAR1 [10]. The demonstration that hypothalamic FFAR1 is regulated by the fasting, as well as by the type of diet, provides further evidence supporting its role as a nutrient sensor and modulator within the hypothalamus in response to nutritional factors.

Next, we explored the mechanisms underlying the body mass reduction promoted by the central action of TUG-905, a potent FFAR1

agonist [17,19]. We showed that TUG-905 did not impact feeding, indicating that this was not the main mechanism explaining body mass reduction when hypothalamic FFAR1 was activated. Importantly, our study revealed that daily ICV treatment with TUG-905 exhibited greater therapeutic potential in inducing body weight reduction, compared to the continuous infusion via central osmotic mini-pumps. In that paradigm, we observed a modest decrease in body weight (data not shown), with a slight increase in energy expenditure, although these changes did not reach statistical significance when analyzed by ANCOVA analysis. The differences in responses between daily bolus administration *vs.* continuous infusion may be likely attributed to long-term receptor desensitization or the development of drug tolerance, thereby limiting the effectiveness of the agonist [41].

Additionally, our findings demonstrated that TUG-905 promoted BAT thermogenesis and the browning of WAT. It is worthwhile mentioning that in other conditions of thermogenesis-induced increase in energy expenditure, there is an increase in food intake. This occurs in cold exposure [42], upon overexpression of either UCP1 or UCP3 [43,44] or
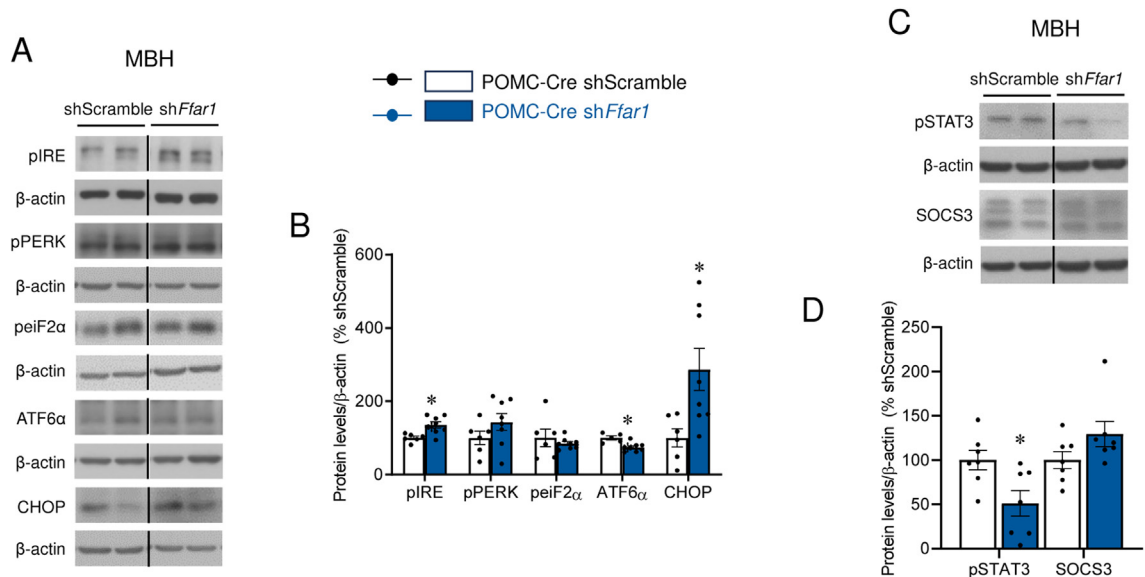
**Figure 7:** Effect of POMC-specific *Ffar1* knockdown on the hypothalamus. (A) Representative immunoblot images and (B) densitometry quantification of protein levels of ER stress markers in the MBH of POMC-Cre mice treated with AAV encoding shScramble or sh*Ffar1* (n = 5−8 mice/group). (C) Representative immunoblot images and (D) densitometry quantification of protein levels of pSTAT3 and SOCS3 in the MBH of POMC-Cre mice treated with AAV encoding shScramble or s*hFfar1* (n = 7 mice/group). Data are expressed as MEAN ± SEM. Statistical significance was determined by t-test; *$P < 0.05$, **$P < 0.01$ *vs.* shScramble.

after thyroid hormone treatments [21,33]. Conversely, under central FFAR1 activation, the thermogenic effect was not accompanied by a compensatory increase in caloric intake, which could be regarded as an additional beneficial effect of this intervention. In fact, it is possible that body mass reduction may result from the combination of increased energy expenditure and unchanged caloric intake.
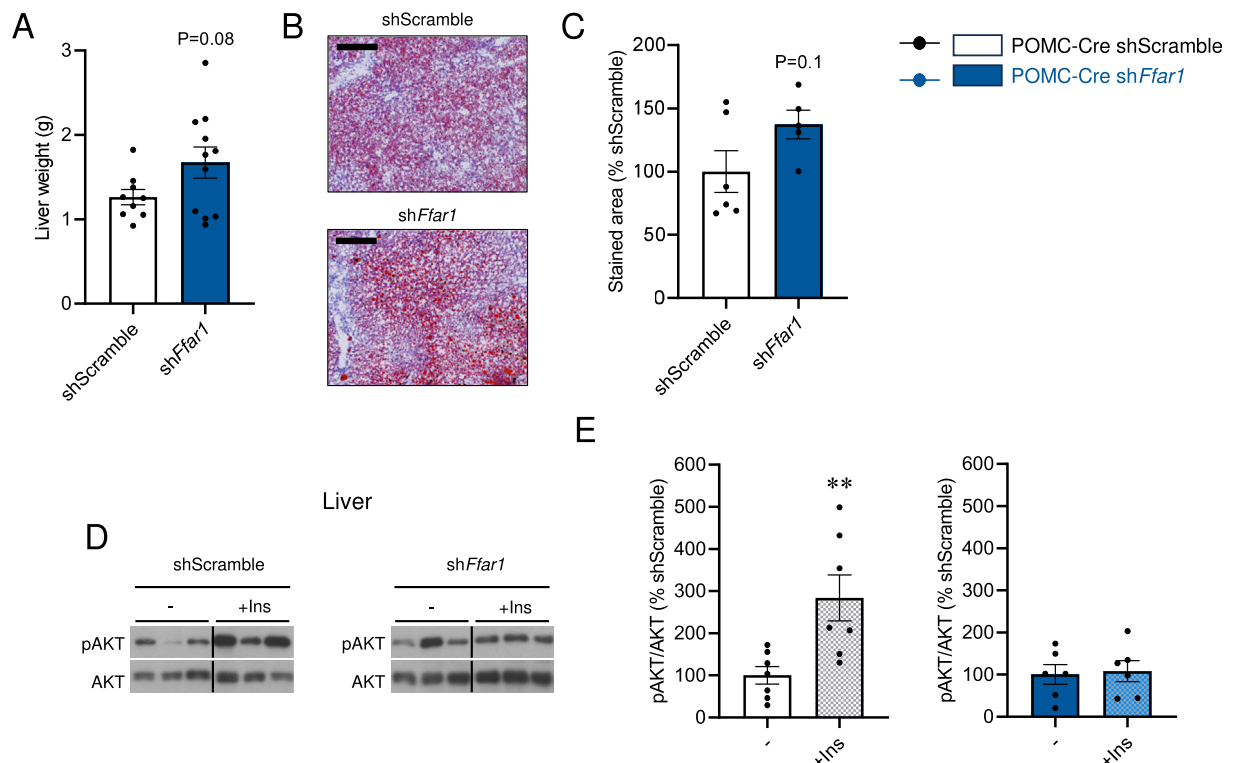


**Figure 8:** Effect of POMC-specific *Ffar1* knockdown on hepatic insulin resistance. (A) Liver weight (n = 9−11 mice/group), (B) representative microphotographs of Oil-Red staining (10X, scale bar: 100 μm) and (C) hepatic lipid content in Oil Red O-stained sections (n = 5−6 mice/group) of POMC-Cre mice treated with AAV encoding shScramble or sh*Ffar1*. (D) Representative immunoblot images and (E) densitometry quantification of hepatic protein levels of pAKT/AKT in the MBH of POMC-Cre mice treated with AAV encoding shScramble or sh*Ffar1*, before (−) and after (+Ins) injection in the cava vein (n = 6−7 mice/group). Data are expressed as MEAN ± SEM. Statistical significance was determined by Student's t-test; **$P < 0.01$ *vs.*−.

Simultaneously with the thermogenic response triggered by FFAR1 activation, we observed a decrease in liver weight and NEFA circulating levels, while TG and cholesterol levels remained unchanged. These findings suggest that the administration of TUG-905 in DIO mice primarily leads to body mass reduction, mainly attributed to increased BAT activity, with mild protective effects on the liver.

It is worth noting that the ICV treatment with TUG-905, while specifically targeting the hypothalamus, lacks cell-specificity in its mechanism of action. By affecting multiple cell types, TUG-905 may exert its effects on various signaling pathways, neural circuits, and molecular targets involved in the hypothalamic regulation of body mass. To further dissect the roles of hypothalamic FFAR1 in the regulation of whole-body energy balance, we selected the melanocortin system to be targeted by the cell-specific targeting of FFAR1. Notably, targeting of FFAR1 in POMC neurons resulted in increased body mass gain due to enhanced caloric intake and reduced hepatic insulin sensitivity, without changes in neither BAT thermogenesis nor in energy expenditure. POMC neurons are components of the first order neurons that sense whole-body energy status and respond promoting signals that control caloric intake, energy expenditure and systemic glucose homeostasis [18,45]. The knockout of *Pomc* specifically in ARC neurons results in hyperphagia and early-onset obesity, even if mice are fed on regular chow [46]; moreover, *Pomc* mutants also exhibit hyperinsulinemia and hepatic steatosis [46]. Thus, there is considerable phenotypic overlap when comparing the ARC *Pomc* knockout with the ARC POMC knockdown of *Ffar1*. POMC neurons are mostly involved in the regulation of food intake and glucose homeostasis; however, there are certain POMC-specific interventions that have resulted in changes in energy expenditure and BAT thermogenesis [47,48]. For quite some time, the diversity and complexity of functions executed by ARC POMC neurons have been a matter of intense investigation [18,45]. The emergence of single-cell transcriptomics has shed some light on this issue, showing that within the ARC POMC neuronal population, there exits several distinct subpopulations, each contributing to essential roles in different sensory and regulatory networks [18,49]. Thus, POMC neurons, with their diverse molecular phenotypes and widespread projections, can provide different physiological responses to changing metabolic needs and endocrine milieu [18,49]. With this concept in mind, we believe that the results we describe in this study could indicate that FFAR1 is present in specific subsets of ARC POMC neurons, likely being those mostly involved in the regulation of feeding and hepatic glucose tolerance. Further studies could provide a more refined dissection of the FFAR1 expression in distinct POMC subpopulations of the ARC. This could explain one conundrum of this study, namely the divergent metabolic phenotypes observed after pharmacological activation with TUG-905 (i.e., increased BAT thermogenesis and EE without major changes in feeding) and genetic silencing of *Ffar1* in POMC neurons (i.e., increased food intake without major changes in EE). Further work by targeting specific subpopulations of POMC neurons will allow to elucidate the precise role of FFAR1 at different hypothalamic sites. Also, the possible role of FFAR1 in other hypothalamic neuronal populations regulating BAT thermogenesis cannot be excluded. In this sense, studies have shown that most of the BAT sympathetic fibers driving the activation of thermogenesis originate in the steroidogenic factor-1 (SF1) system of the VMH [26], and the endocannabinoid system [50]. Specific targeting of FFAR1 in these cell types will help to understand the precise role of this receptor in the central control of energy balance.

## 5. CONCLUSIONS

In summary, this study offers compelling evidence showing that hypothalamic FFAR1 plays a pivotal role in regulating energy metabolism potentially by influencing POMC neurons. Further research identifying the different neuronal subsets though which FFAR1 exerts its influence could lead the development of more precise therapeutic approaches for addressing obesity and related metabolic disorders.

## AUTHOR CONTRIBUTIONS

NRVD, EM, AE-S, DB, VC, EN, and MF performed the in vivo experiments and analytical methods.
RH-T and MC performed the RNAscope analyses.
PGG and JLL-G performed the HPLC analyses.
ERU and TU provided the TUG-905.
NRVD, LAV and ML developed the hypothesis, conceived, and designed the experiments.
NRVD and ML analyzed the data.
NRVD, IGG, OB, CD, RN, JLL-G, MC, LAV and ML interpreted, and discussed the data.
NRVD and ML made the figures.
NRVD, LAV and ML wrote the manuscript.
All authors revised and edited the manuscript.
LAV and ML secured funding and supervised the work.
ML is the lead contact.

## ACKNOWLEDGMENTS

## DECLARATION OF COMPETING INTEREST

The authors declare that they have no known competing financial interests or personal relationships that could have appeared to influence the work reported in this paper.

## DATA AVAILABILITY

Excel file with the data has been submitted.

# Original Article

## REFERENCES

[1] Briscoe CP, Tadayyon M, Andrews JL, Benson WG, Chambers JK, Eilert MM, et al. The orphan G protein-coupled receptor GPR40 is activated by medium and long chain fatty acids. J Biol Chem 2003;278(13):11303—11.

[2] Itoh Y, Kawamata Y, Harada M, Kobayashi M, Fujii R, Fukusumi S, et al. Free fatty acids regulate insulin secretion from pancreatic beta cells through GPR40. Nature 2003;422(6928):173—6.

[3] Schroder R, Schmidt J, Blattermann S, Peters L, Janssen N, Grundmann M, et al. Applying label-free dynamic mass redistribution technology to frame signaling of G protein-coupled receptors noninvasively in living cells. Nat Protoc 2011;6(11):1748—60.

[4] Hauge M, Vestmar MA, Husted AS, Ekberg JP, Wright MJ, Di Salvo J, et al. GPR40 (FFAR1) — combined Gs and Gq signaling in vitro is associated with robust incretin secretagogue action ex vivo and in vivo. Mol Metab 2015;4(1):3—14.

[5] Mancini AD, Bertrand G, Vivot K, Carpentier E, Tremblay C, Ghislain J, et al. Beta-arrestin recruitment and biased agonism at free fatty acid receptor 1. J Biol Chem 2015;290(34):21131—40.

[6] Rives ML, Rady B, Swanson N, Zhao S, Qi J, Arnoult E, et al. GPR40-Mediated Galpha12 activation by allosteric full agonists highly efficacious at potentiating glucose-stimulated insulin secretion in human islets. Mol Pharmacol 2018;93(6):581—91.

[7] Peng XV, Marcinak JF, Raanan MG, Cao C. Combining the G-protein-coupled receptor 40 agonist fasiglifam with sitagliptin improves glycaemic control in patients with type 2 diabetes with or without metformin: a randomized, 12-week trial. Diabetes Obes Metab 2017;19(8):1127—34.

[8] Kaku K, Araki T, Yoshinaka R. Randomized, double-blind, dose-ranging study of TAK-875, a novel GPR40 agonist, in Japanese patients with inadequately controlled type 2 diabetes. Diabetes Care 2013;36(2):245—50.

[9] Nishizaki H, Matsuoka O, Kagawa T, Kobayashi A, Watanabe M, Moritoh Y. SCO-267, a GPR40 full agonist, stimulates islet and gut hormone secretion and improves glycemic control in humans. Diabetes 2021;70(10):2364—76.

[10] Dragano NRV, Solon C, Ramalho AF, de Moura RF, Razolli DS, Christiansen E, et al. Polyunsaturated fatty acid receptors, GPR40 and GPR120, are expressed in the hypothalamus and control energy homeostasis and inflammation. J Neuroinflammation 2017;14(1):91.

[11] Ma D, Tao B, Warashina S, Kotani S, Lu L, Kaplamadzhiev DB, et al. Expression of free fatty acid receptor GPR40 in the central nervous system of adult monkeys. Neurosci Res 2007;58(4):394—401.

[12] Nascimento LF, Souza GF, Morari J, Barbosa GO, Solon C, Moura RF, et al. n-3 fatty acids induce neurogenesis of predominantly POMC-expressing cells in the hypothalamus. Diabetes 2016;65(3):673—86.

[13] Engel DF, Bobbo VCD, Solon CS, Nogueira GA, Moura-Assis A, Mendes NF, et al. Activation of GPR40 induces hypothalamic neurogenesis through p38- and BDNF-dependent mechanisms. Sci Rep 2020;10(1):11047.

[14] Dragano NR, Monfort-Pires M, Velloso LA. Mechanisms MEDIATING the actions of fatty acids in the hypothalamus. Neuroscience 2020;447:15—27.

[15] Lopez M, Nogueiras R, Tena-Sempere M, Dieguez C. Hypothalamic AMPK: a canonical regulator of whole-body energy balance. Nat Rev Endocrinol 2016;12(7):421—32.

[16] Lopez M. Hypothalamic AMPK as a possible target for energy balance-related diseases. Trends Pharmacol Sci 2022;43(7):546—56.

[17] Hudson BD, Shimpukade B, Mackenzie AE, Butcher AJ, Pediani JD, Christiansen E, et al. The pharmacology of TUG-891, a potent and selective agonist of the free fatty acid receptor 4 (FFA4/GPR120), demonstrates both potential opportunity and possible challenges to therapeutic agonism. Mol Pharmacol 2013;84(5):710—25.

[18] Quarta C, Claret M, Zeltser LM, Williams KW, Yeo GSH, Tschop MH, et al. POMC neuronal heterogeneity in energy balance and beyond: an integrated view. Nat Metab 2021;3(3):299—308.

[19] Christiansen E, Due-Hansen ME, Urban C, Grundmann M, Schroder R, Hudson BD, et al. Free fatty acid receptor 1 (FFA1/GPR40) agonists: mesyl-propoxy appendage lowers lipophilicity and improves ADME properties. J Med Chem 2012;55(14):6624—8.

[20] Rial-Pensado E, Freire-Agulleiro O, Rios M, Guo DF, Contreras C, Seoane-Collazo P, et al. Obesity induces resistance to central action of BMP8B through a mechanism involving the BBSome. Mol Metab 2022;59:101465.

[21] Martinez-Sanchez N, Seoane-Collazo P, Contreras C, Varela L, Villarroya J, Rial-Pensado E, et al. Hypothalamic AMPK-ER stress-JNK1 axis mediates the central actions of thyroid hormones on energy balance. Cell Metab 2017;26(1):212—229 e212.

[22] Milbank E, Dragano NRV, Gonzalez-Garcia I, Garcia MR, Rivas-Limeres V, Perdomo L, et al. Small extracellular vesicle-mediated targeting of hypothalamic AMPKalpha1 corrects obesity through BAT activation. Nat Metab 2021;3(10):1415—31.

[23] Seoane-Collazo P, Rial-Pensado E, Estevez-Salguero A, Milbank E, Garcia-Caballero L, Rios M, et al. Activation of hypothalamic AMP-activated protein kinase ameliorates metabolic complications of experimental arthritis. Arthritis Rheumatol 2022;74(2):212—22.

[24] Gonzalez-Garcia I, Contreras C, Estevez-Salguero A, Ruiz-Pino F, Colsh B, Pensado I, et al. Estradiol regulates energy balance by ameliorating hypothalamic ceramide-induced ER stress. Cell Rep 2018;25(2):413—423 e415.

[25] Gonzalez-Rellan MJ, Fondevila MF, Fernandez U, Rodriguez A, Varela-Rey M, Veyrat-Durebex C, et al. O-GlcNAcylated p53 in the liver modulates hepatic glucose production. Nat Commun 2021;12(1):5068.

[26] Seoane-Collazo P, Roa J, Rial-Pensado E, Linares-Pose L, Beiroa D, Ruiz-Pino F, et al. SF1-Specific AMPKalpha1 deletion protects against diet-induced obesity. Diabetes 2018;67(11):2213—26.

[27] Gonzalez-Garcia I, Freire-Agulleiro O, Nakaya N, Ortega FJ, Garrido-Gil P, Linares-Pose L, et al. Olfactomedin 2 deficiency protects against diet-induced obesity. Metabolism 2022;129:155122.

[28] Seoane-Collazo P, Linares-Pose L, Rial-Pensado E, Romero-Pico A, Moreno-Navarrete JM, Martinez-Sanchez N, et al. Central nicotine induces browning through hypothalamic kappa opioid receptor. Nat Commun 2019;10(1):4037.

[29] Martinez-Sanchez N, Moreno-Navarrete JM, Contreras C, Rial-Pensado E, Ferno J, Nogueiras R, et al. Thyroid hormones induce browning of white fat. J Endocrinol 2017;232(2):351—62.

[30] Milbank E, Dragano N, Vidal-Gomez X, Rivas-Limeres V, Garrido-Gil P, Wertheimer M, et al. Small extracellular vesicle targeting of hypothalamic AMPKalpha1 promotes weight loss in leptin receptor deficient mice. Metabolism 2023;139:155350.

[31] Contreras C, Gonzalez-Garcia I, Seoane-Collazo P, Martinez-Sanchez N, Linares-Pose L, Rial-Pensado E, et al. Reduction of hypothalamic endoplasmic reticulum stress activates browning of white fat and ameliorates obesity. Diabetes 2017;66(1):87—99.

[32] Martins L, Seoane-Collazo P, Contreras C, Gonzalez-Garcia I, Martinez-Sanchez N, Gonzalez F, et al. A functional link between AMPK and orexin mediates the effect of BMP8B on energy balance. Cell Rep 2016;16(8):2231—42.

[33] Lopez M, Varela L, Vazquez MJ, Rodriguez-Cuenca S, Gonzalez CR, Velagapudi VR, et al. Hypothalamic AMPK and fatty acid metabolism mediate thyroid regulation of energy balance. Nat Med 2010;16(9):1001—8.

[34] Hauser AS, Attwood MM, Rask-Andersen M, Schioth HB, Gloriam DE. Trends in GPCR drug discovery: new agents, targets and indications. Nat Rev Drug Discov 2017;16(12):829—42.

[35] Alquier T, Peyot ML, Latour MG, Kebede M, Sorensen CM, Gesta S, et al. Deletion of GPR40 impairs glucose-induced insulin secretion in vivo in mice without affecting intracellular fuel metabolism in islets. Diabetes 2009;58(11): 2607—15.

[36] Li Z, Xu X, Huang W, Qian H. Free fatty acid receptor 1 (FFAR1) as an emerging therapeutic target for type 2 diabetes mellitus: recent progress and prevailing challenges. Med Res Rev 2018;38(2):381—425.

[37] Al-Massadi O, Dieguez C, Schneeberger M, Lopez M, Schwaninger M, Prevot V, et al. Multifaceted actions of melanin-concentrating hormone on mammalian energy homeostasis. Nat Rev Endocrinol 2021;17(12): 745—55.

[38] Moura-Assis A, Friedman JM, Velloso LA. Gut-to-brain signals in feeding control. Am J Physiol Endocrinol Metab 2021;320(2):E326—32.

[39] Lam TK, Pocai A, Gutierrez-Juarez R, Obici S, Bryan J, Aguilar-Bryan L, et al. Hypothalamic sensing of circulating fatty acids is required for glucose homeostasis. Nat Med 2005;11(3):320—7.

[40] Obici S, Feng Z, Arduini A, Conti R, Rossetti L. Inhibition of hypothalamic carnitine palmitoyltransferase-1 decreases food intake and glucose production. Nat Med 2003;9(6):756—61.

[41] Rajagopal S, Shenoy SK. GPCR desensitization: acute and prolonged phases. Cell Signal 2018;41:9—16.

[42] Ravussin Y, Xiao C, Gavrilova O, Reitman ML. Effect of intermittent cold exposure on brown fat activation, obesity, and energy homeostasis in mice. PLoS One 2014;9(1):e85876.

[43] Clapham JC, Arch JR, Chapman H, Haynes A, Lister C, Moore GB, et al. Mice overexpressing human uncoupling protein-3 in skeletal muscle are hyperphagic and lean. Nature 2000;406(6794):415—8.

[44] Bernal-Mizrachi C, Weng S, Li B, Nolte LA, Feng C, Coleman T, et al. Respiratory uncoupling lowers blood pressure through a leptin-dependent mechanism in genetically obese mice. Arterioscler Thromb Vasc Biol 2002;22(6):961—8.

[45] Toda C, Santoro A, Kim JD, Diano S. POMC neurons: from birth to death. Annu Rev Physiol 2017;79:209—36.

[46] Bumaschny VF, Yamashita M, Casas-Cordero R, Otero-Corchon V, de Souza FS, Rubinstein M, et al. Obesity-programmed mice are rescued by early genetic intervention. J Clin Investig 2012;122(11):4203—12.

[47] Yao T, Deng Z, Gao Y, Sun J, Kong X, Huang Y, et al. Ire1alpha in pomc neurons is required for thermogenesis and glycemia. Diabetes 2017;66(3): 663—73.

[48] Xiao Y, Deng Y, Yuan F, Xia T, Liu H, Li Z, et al. ATF4/ATG5 signaling in hypothalamic proopiomelanocortin neurons regulates fat mass via affecting energy expenditure. Diabetes 2017;66(5):1146—58.

[49] Campbell JN, Macosko EZ, Fenselau H, Pers TH, Lyubetskaya A, Tenen D, et al. A molecular census of arcuate hypothalamus and median eminence cell types. Nat Neurosci 2017;20(3):484—96.

[50] Cardinal P, Bellocchio L, Clark S, Cannich A, Klugmann M, Lutz B, et al. Hypothalamic CB1 cannabinoid receptors regulate energy balance in mice. Endocrinology 2012;153(9):4136—43.